High-Pressure Hydrogen Adsorption on a Porous Electron-Rich Covalent Organonitridic Framework

Maxwell Murialdo*[1], Nicholas J. Weadock[2], Yiqun Liu[3], Channing C. Ahn[2], Sarah E. Baker[1], Kai Landskron[3], Brent Fultz[2]

1. Lawrence Livermore Natl Lab, Livermore, CA USA
2. California Institute of Technology, W.M. Keck Lab, Pasadena, CA 91125 USA.
3. Lehigh Univ, Dept Chem, Bethlehem, PA 18015 USA.

Supporting Information

* Corresponding Author Email: maxmurialdo@gmail.com

Table of Contents

1. Material Synthesis

A porous, electron-rich, covalent, organonitridic framework (PECONF-4) was produced from inexpensive 3,3'-diaminobenzidine (DAB) and hexachlorocyclotriphosphazene in a simple polycondensation reaction with dimethylsulphoxide (DMSO) as the solvent. Due to its four amino groups, DAB serves as an electron-rich building block while hexachlorocyclotriphosphazene[1, 2] serves as the nitridic building unit. These building blocks cost significantly less than those typically used to synthesize covalent organic frameworks. The materials were acquired as monoliths that could be dried or solvent-exchanged without cracking or disintegrating and could be modified by altering the quantity of solvent (DMSO) in the mixture. The full synthesis procedure has been detailed elsewhere.[3]

2. Experimental Methods

Ultra-high purity (UHP) nitrogen (99.999%) was obtained from Airgas and nitrogen adsorption isotherms were measured at 77 K up to 0.1 MPa using a Micromeritics Tristar II 3020 apparatus. Using supercritical fluid chromatography (SFC) grade carbon dioxide (99.995%) from Air Liquide America Corporation and UHP argon (99.999%) from Airgas, adsorption isotherms were measured at 298 and 87K respectively on a custom Sieverts apparatus designed and tested for accuracy up to 10 MPa.[4-6] High-pressure UHP hydrogen (99.999%, from Airgas) adsorption isotherms were

measured at 77, 87, 253, 273, and 298K at pressures of up to 9 MPa on the custom Sieverts apparatus.

The Sieverts apparatus was equipped with a molecular drag pump capable of achieving a vacuum of 10^{-10} MPa. Prior to testing, each sample was loaded and degassed at 473K under a vacuum of less than 10^{-9} MPa, as validated by a digital cold cathode pressure sensor (I-MAG, Series 423). For these measurements, PECONF-4 was loaded into a stainless-steel reactor sealed with a copper gasket. Low temperatures isotherms were measured by submersing the reactor in a cryogenic bath of liquid nitrogen or liquid argon, or a chiller bath with temperature feedback control. The reactor temperature was monitored with K-type thermocouples and temperature fluctuations were maintained to within $\pm$ 0.1 K of the set temperature. The temperature of the gas manifold was verified with platinum resistance thermometers. Multiple adsorption/desorption isotherms were taken to ensure reversibility and the error between identical trials was found to be less than 1%.

3. Skeletal Density

PECONF-4 was found to have a skeletal density of 1.484 $\pm$0.008 g mL^{-1} by helium pycnometry. This value is lower than the skeletal density of most superactivated carbons (~2.1 g mL^{-1}).

4. Pore-Size Distribution

The pore-size distribution of PECONF-4 was determined from CO_2 adsorption analyzed with density functional theory. No macropores or mesopores were observed in PECONF-4 and the micropores are predominantly less than 7 angstroms in width. The pore-size distribution has distinct peaks at widths of approximately 4.5, 5.3 and 6.0 Angstroms (Figure S1). At cryogenic temperatures, qualitatively slow gas adsorption/desorption was observed, likely owing to limited gas transport in the small pores of PECONF-4. For comparison a sample of PECONF-4 was pulverized to destroy any monolithic structural barriers, but the gas adsorption isotherms remained unaffected.

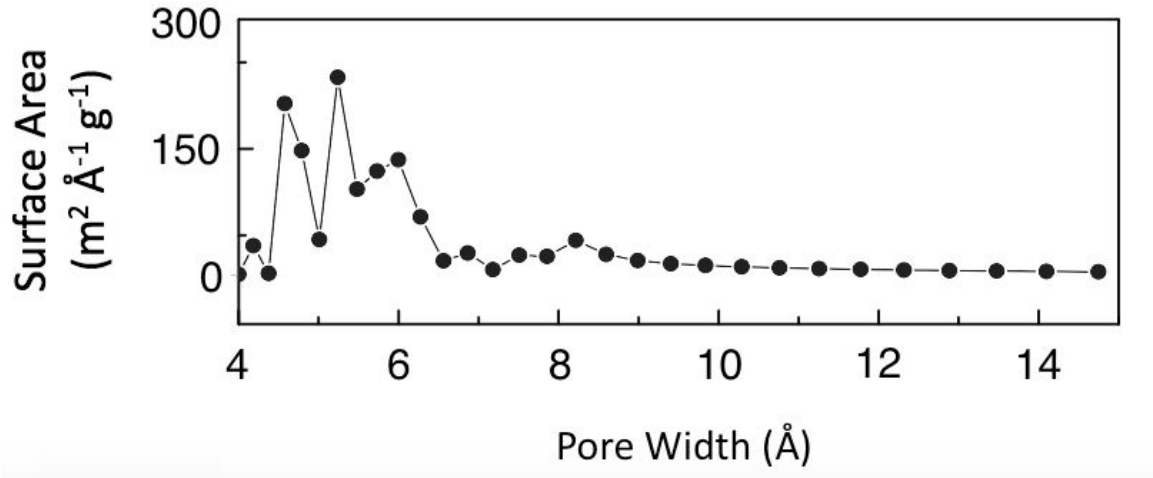

Figure S1. The pore size distribution of PECONF-4

5. Transmission Electron Microscopy

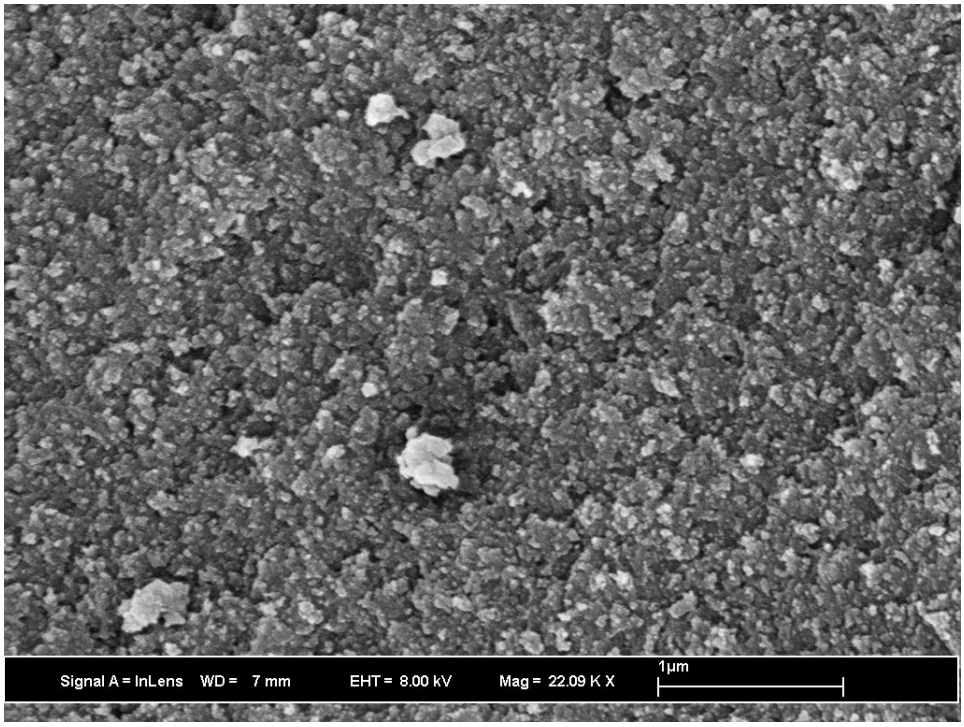

Figure S2. Transmission electron microscope image of PECONF-4

6. MAS NMR Spectroscopy

^{13}C and ^{31}P CP MAS NMR spectra were taken of PECONF-4. Strong ^{13}C CP MAS NMR signals at 141 and 131 p.p.m., along with a weaker signal at 106 p.p.m., and a shoulder at 121 p.p.m., are consistent with the 3,3'-diaminobenzidine building block. A signal at 39 p.p.m. is indicative of residual dimethyl-sulphoxide solvent. The ^{31}P CP MAS NMR data has peaks between 0 and -25 p.p.m., typical for $P(V)N_4$ tetrahedra. The sharpness of the peaks suggests a high degree of order (for a non-crystalline sample). We have summarized these results in prior work.[3]

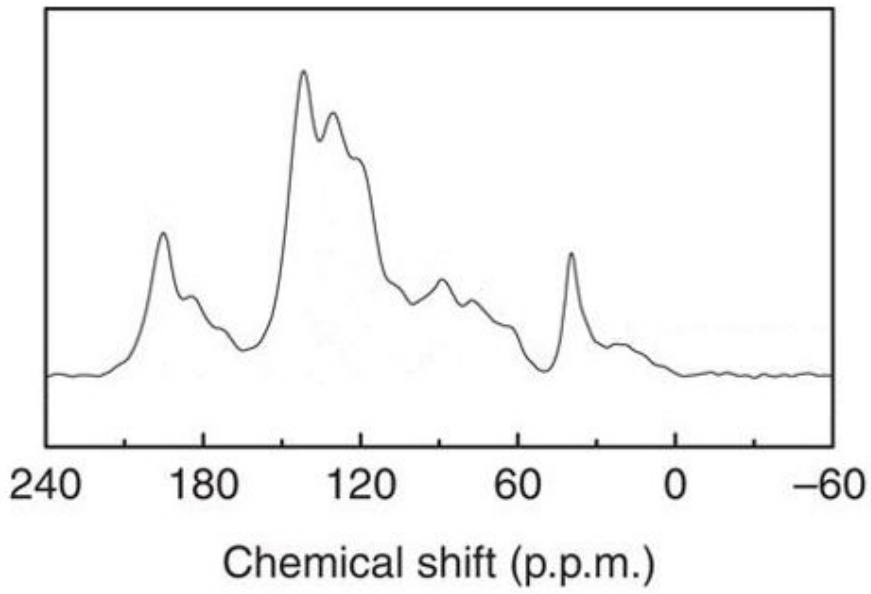

Figure S3. ^{13}C CP MAS NMR spectroscopy on PECONF-4 (taken at 75.468 MHz and referenced to the downfield line of adamantine at 38.55 p.p.m.)

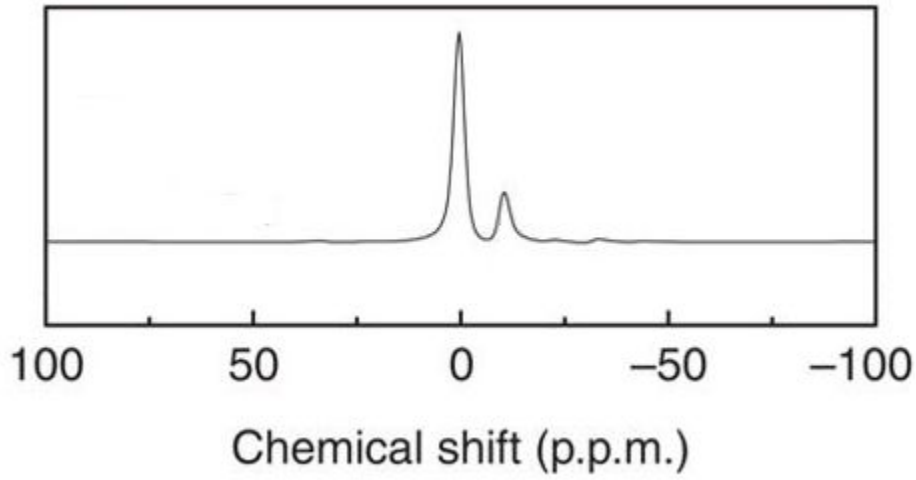

Figure S4. ^{31}P CP MAS NMR spectroscopy on PECONF-4 (taken at 75.468 MHz, chemical shift of 85% H_3PO_4 set to zero)

7. X-Ray Diffraction

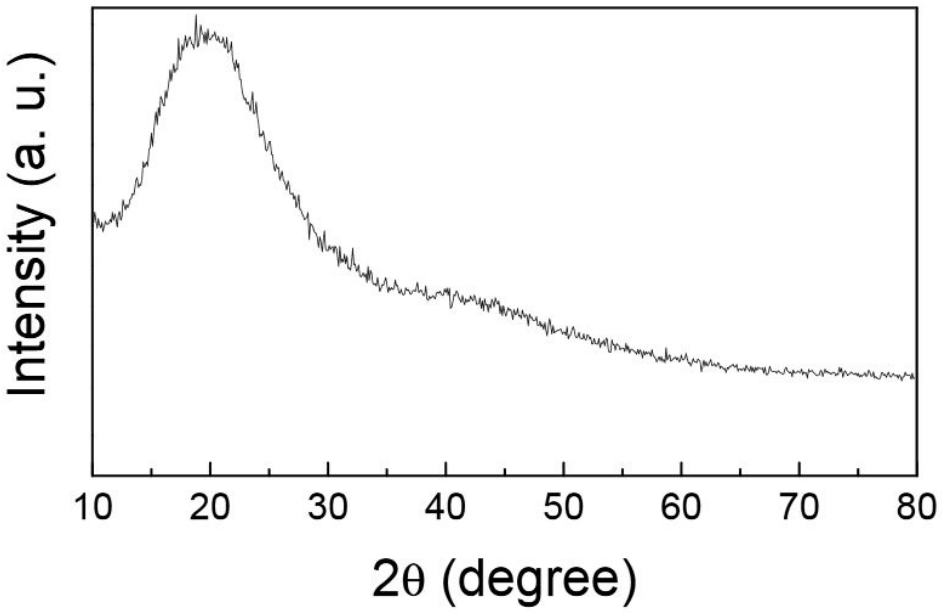

Figure S5. X-ray diffraction indicates that PECONF-4 is non-crystalline (Cu Kα radiation source, λ = 0.15405 nm).

8. Fourier Transform Infrared Spectroscopy

PECONF-4 has a broad band around 3,420 cm^{-1} along with a sharp band near 1,617 cm^{-1}, due to N-H stretching and bending vibrations, respectively. Additional broad bands around 1,090 cm^{-1} and 950 cm^{-1} are due to v_{as}(P-NH-P) vibrations, while the band at 520 cm^{-1} indicates δ(P=N-P) vibrations. Bands around 1,218 and 1,420 cm^{-1} indicate v_{as}(P=N-P) vibrations. We have summarized these results in our prior work.[3]

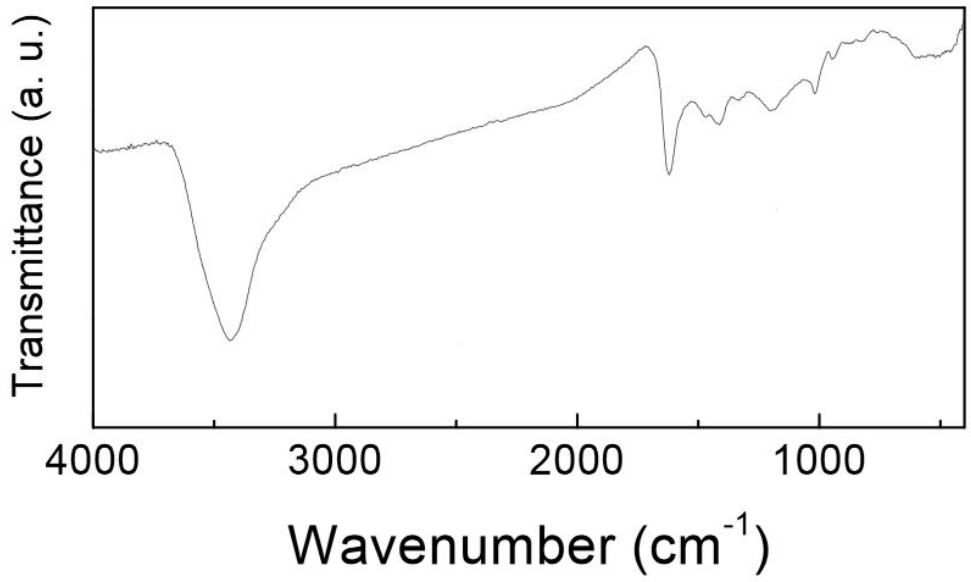

Figure S6. The FT-IR spectrum of PECONF-4

9. Differential Thermogravimetry and Thermogravimetric Analysis

PECONF-4 was found to be stable to above 400 °C in air and to above 600 °C in N_2. Mass losses below 300 °C are attributed to the desorption of small quantities of water and occluded DMSO. Around 500 °C, the organic units undergo oxidation (in air). Around 700 °C the P-N units undergo decomposition. We have summarized these results

in prior work (where differential thermogravimetry and thermogravimetric analysis plots of PECONF-4 are published).[3]

10. The BET Method, Its Limitations and Applicability

While it has been shown that BET theory does not accurately model adsorption phenomena in any physically known gas-solid systems,[7] the BET method provides a reasonable estimate of specific surface area (as corroborated by computational studies)[8, 9] and is one of the most important metrics in comparing adsorbents.

Severe limitations exist in any attempt to measure the BET specific surface area of a microporous material (pores less than 20 Angstroms). These limitations are described in detail by Rouquerol et al. and largely derive from the fact that small micropores allow overlapping wall potentials to interact with the adsorbate, leading to increased micropore filling.[7] In general this leads to an overestimation of BET surface area in microporous materials.[10, 11] Nonetheless, it is standard practice to apply BET analysis to microporous materials (with caveats), and a number of studies corroborate the efficacy of BET measurements on microporous materials despite theoretical objections.[7, 8, 12] BET analysis on microporous materials forms the bulk of the empirical evidence for Chahine's rule.[13-15] Bae et al. have further shown that BET analysis may be applied to ultramicropores (less than 7 angstroms in diameter) with errors of less than 10%, as long as the region of the isotherm analyzed is constrained by consistency criteria.[9]

The standard BET method is to plot $\frac{\left(P/P_o\right)}{\left(n\left(1-P/P_o\right)\right)}$ versus P/P_o and analyze a linear midsection between $P/P_o = 0.05$ and $P/P_o = 0.35$. Here *P* is pressure, P_o is saturation pressure and *n* is excess adsorption. The slope (S) and y-intercept (I) of this linear region give *C* and n_m, respectively (by Equations S1 and S2).

$$C = \frac{I+S}{I} \quad \text{(S1)}$$

$$n_m = \frac{1}{S+I} \quad \text{(S2)}$$

The parameter *C* is correlated with the strength of the adsorbate-adsorbent interactions and n_m is the monolayer capacity of the adsorbent. The parameter n_m may be multiplied by the cross-sectional area of the probe molecule to determine a specific surface area. However, in micropores the strong overlap of the wall potentials allows adsorbate pore filling at a much lower pressures than in mesopores. Accordingly Rouquerol et al. has suggested additional consistency criteria for determining the appropriate P/P_o interval to analyze.[7] First, *C* must be positive, as a negative value for *C* is non-physical. Second, $n\left(1-P/P_o\right)$ must increase as a function of P/P_o. In this work we have analyzed regions of the BET isotherm corresponding to these consistency criteria. The measured C and n_m parameters are listed in Table S1, along with the P/P_o range of analysis.

	N_2	Ar	CO_2
BET ($m^2\ g^{-1}$)	673±18	676±13	569±2
Range (P/P_o)	0.00940-0.0580	0.000987-0.0999	0.00930-0.167
C Value	1451	1710	74.2
Point B ($m^2\ g^{-1}$)	534+9	N/A	673±4

Table S1. Specific surface areas and parameters

11. The Point B Method for Determining Specific Surface Area

In addition to the BET method, the Point B method was used to redundantly assess specific surface area of PECONF-4. For each PECONF-4 adsorption isotherm (nitrogen at 77K and carbon dioxide at 298K), the nearly linear middle region of the isotherm was identified graphically. The beginning point of this region was estimated and denoted Point B, which should correspond to the point where single layer adsorption transitions to multilayer adsorption accompanied by a decrease in isosteric heat.[7] This estimated monolayer coverage was then converted into an estimated specific surface area for comparison (Table S1).

12. Dual-Langmuir Fitting

In this work we fitted the measured excess adsorption isotherms at multiple temperatures with a superposition of Langmuir isotherms. We developed this fitting technique in prior works and have demonstrated its efficacy for methane[16], ethane[17], carbon dioxide[18], and krypton[19] adsorption on microporous materials. It is an adaptation of the fitting technique published by Mertens[20] and has numerous advantages over simpler fitting techniques. The Langmuir isotherm derives from a simplified, but physically relevant model of adsorption and is thus not a mathematically arbitrary fitting function. However, as most materials do not have a single homogenous absorbent-adsorbate binding-site energy, a superposition of more than one isotherm is necessary.

We have found that for many adsorbate/adsorbent combinations a superposition of 2 Langmuir isotherms suffices to give a good fit with minimal error and only 7 free parameters.[16]

In short, Gibbs excess adsorption, n_e is given by Equation S3, where n_a is absolute adsorption, V_a is the volume of the adsorption layer, and ρ is the gas-phase density.

$$n_e = n_a - V_a\rho(P,T) \quad \text{(S3)}$$

Here n_a is the unknown that is solved for and V_a is an unknown that is left as an independent fitting parameter as there is no generally accurate method of a priori determining the volume of the adsorption layer. Accordingly, the empirically measured excess adsorption quantities are fitted by Equation S4.

$$n_e(P,T) = n_{max} - V_{max}\rho(P,T)\sum_i \alpha_i\left(\frac{K_iP}{1+K_iP}\right) \quad \text{(S4)}$$

Where n_{max} is the maximum absolute adsorption, which serves as a scaling factor, V_{max} is the maximum volume of the adsorption layer, P and T are the pressure and temperature, α_i are the individual weights of each Langmuir isotherm ($\sum_i \alpha_i = 1$) and K_i are the individual equilibrium constants for each of the i Langmuir isotherms. The K_i are given by an Arrhenius-type equation (Equation S5).

$$K_i = \frac{A_i}{\sqrt{T}}e^{\frac{E_i}{RT}} \quad \text{(S5)}$$

Here A_i is a prefactor, E_i is the binding energy and R is the universal gas constant. We set i=2 to limit the number of fitting parameters to 7, which allows for accurate fits with a

manageable number of fitting parameters. The isosteric heat, q_{st}, was determined using Equation S6.

$$q_{st}(n_a) = T\left(\frac{dP}{dT}\right)(v_g - v_l) \quad \text{(S6)}$$

The isosteric heat is reported as a positive quantity as is convention. The change in volume of the adsorbate upon adsorption is calculated as the difference between the gas phase molar volume v_g and the liquid phase molar volume v_l (from data tables). As the derivative is evaluated at constant absolute adsorption (n_a), not constant excess adsorption, the values computed are true "isosteric heats" not "isoexcess heats". Furthermore, this method avoids the common assumptions that the gas behaves ideally and that the adsorbed-phase volume is negligible, which break down in this high-pressure regime.[15]

13. Dual-Langmuir Fits with Only 77 and 87K Isotherms

For redundant comparison, we calculated the isosteric heats of hydrogen adsorption on PECONF-4 at 77 and 87K by using a superposition of Langmuir isotherms to fit *only* the excess adsorption data measured at 77 and 87K. The resulting low temperature isosteric heats are plotted in Figure S7 and closely resemble the results of Figure 2, which were calculated by fitting the isotherms measured at 77, 87, 253, 273, and 298K.

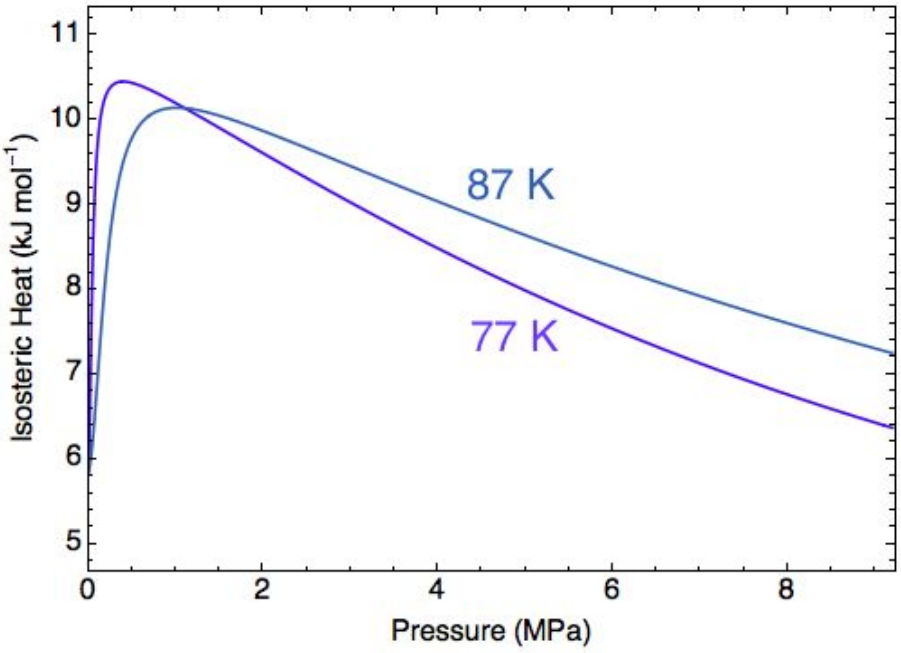

Figure S7. Low temperature isosteric heat of hydrogen on PECONF-4.

14. Method for Estimating Isoexcess Heat of Adsorption without Fitting the Data

Following from the van't Hoff equation, the isoexcess heat of adsorption is determined by calculating the derivative $(1/R)\frac{dln(P)}{d(1/T)}$, while excess adsorption is held constant.[15] When, by coincidence, two data points in an empirically measured dataset correspond to identical amounts of excess adsorption at different temperatures and pressures, the isoexcess heat of adsorption may be calculated for directly, without fitting the data. The results of this method are shown in Figure 3.

References

1. Zhang, M. C.; Li, Y.; Bai, C. Y.; Guo, X. H.; Han, J.; Hu, S.; Jiang, H. Q.; Tan, W.; Li, S. J.; Ma, L. J., Synthesis of Microporous Covalent Phosphazene-Based Frameworks for Selective Separation of Uranium in Highly Acidic Media Based on Size-Matching Effect. *ACS Applied Materials & Interfaces* **2018,** *10* (34), 28936-28947.
2. Li, Z. T.; Zhao, W. N.; Yin, C. Z.; Wei, L. Q.; Wu, W. T.; Hu, Z. P.; Wu, M. B., Synergistic Effects between Doped Nitrogen and Phosphorus in Metal-Free Cathode for Zinc-Air Battery from Covalent Organic Frameworks Coated CNT. *ACS Applied Materials & Interfaces* **2017,** *9* (51), 44519-44528.
3. Mohanty, P.; Kull, L. D.; Landskron, K., Porous covalent electron-rich organonitridic frameworks as highly selective sorbents for methane and carbon dioxide. *Nature Communications* **2011,** *2*, 6.
4. McNicholas, T. P.; Wang, A. M.; O'Neill, K.; Anderson, R. J.; Stadie, N. P.; Kleinhammes, A.; Parilla, P.; Simpson, L.; Ahn, C. C.; Wang, Y. Q.; Wu, Y.; Liu, J., H-2 Storage in Microporous Carbons from PEEK Precursors. *Journal of Physical Chemistry C* **2010,** *114* (32), 13902-13908.
5. Purewal, J. J.; Kabbour, H.; Vajo, J. J.; Ahn, C. C.; Fultz, B., Pore size distribution and supercritical hydrogen adsorption in activated carbon fibers. *Nanotechnology* **2009,** *20* (20), 6.
6. Purewal, J.; Liu, D. G.; Sudik, A.; Veenstra, M.; Yang, J.; Maurer, S.; Muller, U.; Siegel, D. J., Improved Hydrogen Storage and Thermal Conductivity in High-Density MOF-5 Composites. *Journal of Physical Chemistry C* **2012,** *116* (38), 20199-20212.
7. Rouquerol Françoise; Rouquerol, J.; Sing, K. S. W.; Llewellyn, P. L.; Maurin, G. *Adsorption by powders and porous solids: principles, methodology and applications*; Elsevier/AP: Amsterdam, 2014.
8. Walton, K. S.; Snurr, R. Q., Applicability of the BET method for determining surface areas of microporous metal-organic frameworks. *Journal of the American Chemical Society* **2007,** *129* (27), 8552-8556.
9. Bae, Y. S.; Yazaydin, A. O.; Snurr, R. Q., Evaluation of the BET Method for Determining Surface Areas of MOFs and Zeolites that Contain Ultra-Micropores. *Langmuir* **2010,** *26* (8), 5475-5483.
10. Kaneko, K.; Ishii, C., Superhigh surface-area determination of microporous solids. *Colloids and Surfaces* **1992,** *67*, 203-212.
11. Matsuoka, K.; Yamagishi, Y.; Yamazaki, T.; Setoyama, N.; Tomita, A.; Kyotani, T., Extremely high microporosity and sharp pore size distribution of a large surface area carbon prepared in the nanochannels of zeolite Y. *Carbon* **2005,** *43* (4), 876-879.
12. Rouquerol, J.; Llewellyn, P.; Rouquerol, F. *Studies in Surface Science and Catalysis Characterization of Porous Solids VII - Proceedings of the 7th International Symposium on the Characterization of Porous Solids (COPS-VII), Aix-en-Provence, France, 26-28 May 2005* **2007**, 49–56
13. Poirier, E.; Chahine, R.; Bose, T. K., Hydrogen adsorption in carbon nanostructures. *International Journal of Hydrogen Energy* **2001,** *26* (8), 831-835.
14. Panella, B.; Hirscher, M.; Roth, S., Hydrogen adsorption in different carbon nanostructures. *Carbon* **2005,** *43* (10), 2209-2214.
15. Stadie, N. P., Synthesis and thermodynamic studies of physisorptive energy storage materials. Ph.D. Dissertation, California Institute of Technology, Pasadena, CA, 2013.

16. Stadie, N. P.; Murialdo, M.; Ahn, C. C.; Fultz, B., Anomalous Isosteric Enthalpy of Adsorption of Methane on Zeolite-Templated Carbon. *Journal of the American Chemical Society* **2013,** *135* (3), 990-993.
17. Murialdo, M.; Stadie, N. P.; Ahn, C. C.; Fultz, B., Observation and Investigation of Increasing Isosteric Heat of Adsorption of Ethane on Zeolite-Templated Carbon. *Journal of Physical Chemistry C* **2015,** *119* (2), 944-950.
18. Murialdo, M.; Ahn, C. C.; Fultz, B., A Thermodynamic Investigation of Adsorbate-Adsorbate Interactions of Carbon Dioxide on Nanostructured Carbons. *Aiche Journal* **2018,** *64* (3), 1026-1033.
19. Murialdo, M.; Stadie, N. P.; Ahn, C. C.; Fultz, B., Krypton Adsorption on Zeolite-Templated Carbon and Anomalous Surface Thermodynamics. *Langmuir* **2015,** *31* (29), 7991-7998.
20. Mertens, F. O., Determination of absolute adsorption in highly ordered porous media. *Surface Science* **2009,** *603* (10-12), 1979-1984.